EXPERIMENTAL STUDY ON CYLINDIRCAL PARTICLE MOVEMENT IN A SLURRY PUMP GUIDE VANE

Xianfang WU[1], Chen SHAO[2]*, Houlin LIU[2], Minggao TAN[2], and Bing QU[3]

[1]School of Energy and Power Engineering, Jiangsu University, Zhenjiang, China

[2]Research Center of Fluid Machinery Engineering and Technology, Jiangsu University, Zhenjiang, China

[3]Shandong Xinchuan Mining Mechanical and Electrical Equipment Co., Ltd, Jining, China

*Corresponding author; E-mail: 2112111009@stmail.ujs.edu.cn

To investigate the movement characteristics of cylindrical particles within a slurry pump, the particle trajectories, particle distributions, particle velocity, and passing time of particles in the guide vane are tested by high-speed photography. The test results indicate that the pump performance decreases and the wear of the blade pressure side deteriorates with the increase of cylindrical particle densities. The particles primarily flow into the guide vanes from the suction side and flow out from the pressure side. The velocity loss of particles in the guide vanes increases, and the time for particles passing through the guide vanes increases with particle densities. As the cylindrical particle concentrations increase, the pump performance decreases, and the wear of the blade pressure side deteriorates. Additionally, the total velocity loss of particles in the guide vane increases, and the time for particles passing through the guide vane increases with concentrations. Compared with spherical particles, the pump performance is better when the pump conveys cylindrical particles, and the cylindrical particles are more likely to wear the middle of the guide vane flow channel. The particles mainly flow into the guide vanes from the suction side and flow out from the pressure side. And the velocity loss of cylindrical particles in the guide vane is smaller than that of the spherical particles. The time of cylindrical particles passing through the guide vane is shorter than that of the spherical particles.

Key words**:** *Slurry pump, High-speed photography, Cylindrical particles, Particle trajectory, Particle distribution, Particle velocity*

1. Introduction

With the increasing demand for natural resources and the gradual depletion of land resources, the research and development of deep-sea mining technology has become a hot topic worldwide. With high comprehensive performance, the hydraulic pipeline lifting system of slurry pumps has a broad development prospect [1]. However, as a solid-liquid two-phase flow pump, the efficiency of the slurry pump is significantly affected by submarine mine particle shape, density, and concentration.

Therefore, it is crucial to investigate the motion characteristics of particles to provide a reference for the design and optimization of slurry pumps.

In the past, scholars in the field of solid-liquid two-phase flow mainly focused on fine granules [2-6]. Recently, due to the requirements of practical engineering, the study on large-diameter particles in solid-liquid two-phase flow has received more attention. Beauchesne *et al.* [7] developed a numerical solver for deep-sea ore transport based on the Lagrange method, and the method was suitable for the numerical simulation of large particles. Sakano *et al.* [8] investigated pressure loss in a riser pipe for large particle slurry transport, and the results showed that the peak of pressure loss decreased with the increase of particle densities. Masanobu *et al.* [9] studied large particle motion characteristics in the pipe under different angles. The research found that the collision number between the wall and the particles in the horizontal pipe was large, and in the vertical pipe was small. Ghosh [10] investigated the efficiency of a slurry pump pipe under different sizes, and the results showed that the lifting time reduced with the decrease of particle sizes under the same particle mass of and the pump flow rate. Deng *et al.* [11] conducted experimental and numerical simulation studies on the six-stage slurry pump. It was found that the particle motion in the pump became stable with the increase of flow rates. Hu *et al.* [12] analyzed the slurry pump performance under extreme conditions. The results showed that the pump still had good conveying and certain backflow ability. Tan *et al.* [13] considered the special operating conditions, such as accident shutdown or sudden power failure of a slurry pump, and found that the particle distribution under runaway conditions was more disordered than the nominal flow rate. Hu *et al.* [14] investigated the reflux characteristics of spherical particles in a pump, and it was found the maximum particle diameter should be controlled within 30mm to ensure equipment safety. Guan *et al.* [15] analyzed the reflux characteristics of particles with different shapes in a slurry pump. The results showed that the smaller the sphericity of the non-spherical particles was, the worse the reflux performance was. Sun *et al.* [16] used the DPM (Discrete Phase Model) to study the wear characteristics of a slurry pump under different particle sizes. The research found that the wear of particles on the rotating components increased as the particle size increased. Wang *et al.* [17] tested the particle motion characteristics in the impeller of a two-stage slurry pump. The results showed that the particle passing ability increased as the cross-sectional area of the impeller increased. Luo *et al.* [18] investigated the trajectories of quartz sand with a particle size of 3mm in the guide vane. It was found that the collision position of the particles was mainly at the blade of the inlet and the middle of the guide vane. Wu *et al.* [19] studied the collision characteristics of spherical particles with different physical parameters in the slurry pump. The experimental results showed that the collision probability between the particles and the inlet of the guide vane blade increased with particle size and decreased with the increase of particle density.

Above all, it can be seen that there are relatively few studies on non-spherical particles in slurry pumps by experimental methods, and the motion characteristics of particles in pumps are not fully revealed. In this paper, the visual experiment is used to study the particle trajectories, velocity, and time of cylindrical particles passing through the guide vanes under different particle densities. The concentrations and the motion law of spherical and cylindrical particles in the guide vane are compared.

2. Test models and methods

2.1. Test system

Figure 1 is the diagram of the slurry pump test system structure. To ensure the test accuracy, the measurement errors of the system are analyzed. The primary sensor equipment for the test is flowmeters, pressure transmitters, and torque meters. The pump head and torque errors obtained after the repeatability test were ± 0.953 % and ± 0.421 %, respectively. The results prove the stability and reliability of the test system are satisfied.

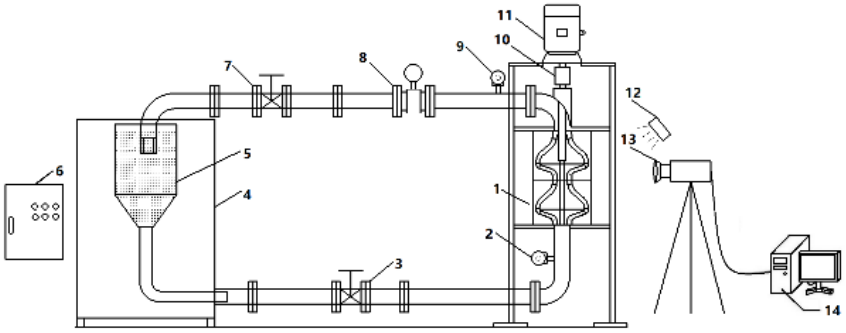

1 Test model pump, 2 Pump inlet pressure transmitter, 3 Pump inlet ball valve, 4 Storage tank motor, 5 Feeding funnel, 6 Frequency conversion cabinet, 7 Pump outlet ball valve, 8 Flowmeter, 9 Pump outlet pressure transmitter, 10 Torque meter, 11 Motor, 12 LED lamp, 13 High-speed photography, 14 Computer control system

Figure 1. Experimental device

2.2. Pump model

The two-stage pump is selected as the research object. The main design parameters of the pump are nominal flow rate Q_d = 82m^3·h^{-1}, pump head H = 20m, and rotating speed n = 960r·min^{-1}. To facilitate the high-speed camera to visualize the solid-liquid two-phase flow of coarse particles, the impeller, and space guide vane are all made of polymethyl methacrylate with good transparency and high hardness [20]. The pump model is shown in Fig. 2. The main structure parameters of the impeller and space guide vane are shown in Table 1.

(a) Impeller (b) guide vane (c) Pump model

Figure 2. Test pump model

Table 1. Pump model structure parameters

	Structure	Parameter
Impeller	Inlet diameter (mm)	126
	Outlet diameter (mm)	300
	Hub diameter (mm)	66
	Blade number	4
	Outlet width (mm)	20
Guide vane	Internal flow line (mm)	300
	Outflow line (mm)	347
	Axial length (mm)	180
	Blade number	5

2.3. Test schemes and the particle model

The coarse particles selected in the visualization test are spherical and cylindrical particles produced by customization. The particle is produced by the method of mold marking and casting. The materials of the particles are silica gel and rubber, respectively. The silica gel color is milky white, density is 1250kg·m^{-3}; the rubber color is black, and the density is 1500kg·m^{-3} and 1800kg·m^{-3}. To ensure the unity of the test variables, the volume of the cylindrical particle is the same as that of the spherical particle [21]. The spherical particle size used in the test is 8mm, and the bottom surface diameter *d* and height *h* of the cylindrical particles are 5.5mm and 11mm, respectively. Particles with different shapes in the test are shown in Fig. 3, and particle test schemes with different physical properties are shown in Table 2.

(a) Spherical particle (b) Cylindrical particle

Figure 3. Particle shape

Table 2. Particles with different physical parameters

Schemes	Shape	Size (mm)	Density (kg·m^{-3})	Concentration (%)
1	Cylindrical	5.5:11	1250, 1500, 1800	3
2	Cylindrical	5.5:11	1500	1, 3, 5
3	Spherical	8	1500	3
	Cylindrical	5.5:11		

2.4. Data processing

2.4.1 Particle trajectories data

A high-speed photography system is used to store the shooting data and record the motion characteristics of particles in the guide vane, and 1000 pictures are taken per second. The Motion Studio software is used to post-process the captured images. To compare the motion characteristics of particles with different physical properties in the guide vane more intuitively, the pixel coordinates are established for the contour of the single guide vane flow channel, and the centroid coordinates of the

particles are extracted to obtain the motion trajectory of the particles in the guide vane flow channel, as shown in Fig. 4. To investigate the motion characteristics of particles in guide vanes, the coordinate positions of the same particle at different times are recorded, respectively. The coordinate points are connected by lines to form a particle trajectory, and then 200 particle trajectories are drawn. The particle trajectories are shown in Fig. 5.

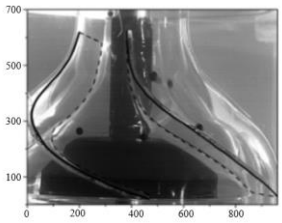

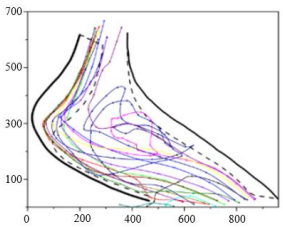

Figure 4. Guide vane flow channel coordinates **Figure 5. Particle trajectories**

According to the particle trajectories in Fig. 5, the single guide vane flow channel is divided into seven areas. First, the inlet is divided into three areas with equal distances, namely area I, area II, and area III (area I is the guide vane inlet near the pressure side, area II is the middle of the guide vane inlet, area III is the suction side of the guide vane inlet). Secondly, a large vortex ring area in the middle of the flow channel is defined as area IV. Finally, the outlet is also divided into equal distances, namely area V, area VI and area VII (area V is the guide vane outlet near the pressure side, area VI is the middle of the guide vane outlet, and area VII is the suction side of the guide vane outlet). The specific range of the guide vane flow channel area is shown in Figure 6. To analyze the particle velocity in the guide vane, the guide vane is divided into six layers, as shown in Fig. 7.

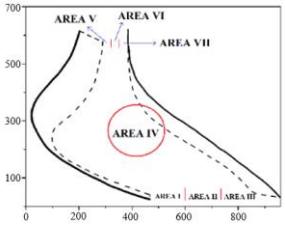

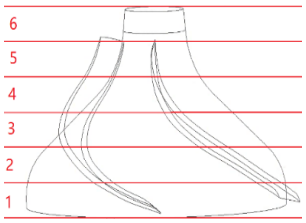

Figure 6. Guide vane flow channel division **Figure 7. Radial division of guide vane**

2.4.2 Pump performance data

When the pump conveys particles, the pump head calculation formula is :

$$H = \Delta Z + \frac{P_{out} - P_{in}}{\left(\rho_p \times C_V + \rho \times \left(1 - C_V\right)\right) g} + \frac{v_2^2 - v_1^2}{2g} \tag{1}$$

In the formula, ΔZ is the height difference between pump inlet and outlet, m. P_{out} is the total pressure at the pump outlet, Pa. P_{in} is the total pressure at the pump inlet, Pa. v_2 is the average velocity at the pump outlet, $m \cdot s^{-1}$. v_1 is the average velocity at the pump inlet, $m \cdot s^{-1}$. ρ_p is the solid phase density, $kg \cdot m^{-3}$. Cv is the solid phase volume fraction.

The formula of solid phase volume fraction is :

$$C_V = \frac{V_p}{V_p + V_f} \tag{2}$$

Where the V_p is the solid phase volume, m^3. V_f is the liquid phase volume, m^3.

The pump efficiency calculation formula is :

$$\eta = \frac{\left(\rho_p \times C_V + \rho \times \left(1 - C_V\right)\right) \times g \times Q \times H}{P} \times 100\% \quad (3)$$

In the formula, g is the acceleration of gravity, $m \cdot s^{-2}$. Q is the inlet flow, $m^3 \cdot h^{-1}$. P is the shaft power, kW.

3. Test result analysis

3.1. Energy performance analysis of pump

Figure 8 illustrates the energy performance of the pump under different particle physical properties. The energy performance trends are consistent in both Fig. 8 (a) and Fig. 8 (b). As shown in Fig. 8 (a), it can be observed that the head and efficiency reduce, and the power increases as the cylindrical particle density increases. In Fig. 8 (b), with the increase of particle concentration, the head and efficiency reduce, and the power increases. It can be found in Fig. 8 (c) that the pump head and efficiency under solid-liquid two-phase flow are lower than that under single-phase. When pump conveys spherical particle two-phase flow, the pump head is reduced by 0.79 %, the efficiency is reduced by 1.27 %, and the power is increased by 0.79 %.

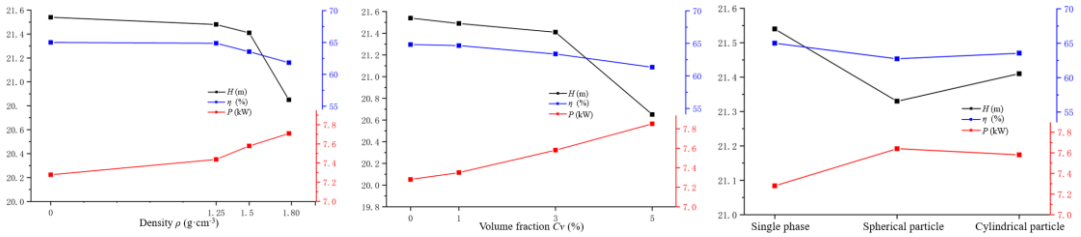

(a) Density **(b) Volume fraction** **(c) Shape**

Figure 8. Energy performance of pump under different physical parameters

3.2. Particle movement law under different densities

3.2.1 Particle trajectories

The particle trajectories (as seen in Fig. 5) entering from different inlets (as seen in Fig. 6) are counted, and the trajectories that appear most frequently are identified and further analyzed as the main particle trajectories. Figure 9 shows the cylindrical particle trajectories under different densities. It can be observed that all the particle trajectories in guide vanes are along the blade pressure side under different densities. From Fig. 9 (a), it is evident that the particle trajectories are more likely move to the blade pressure side when entering the guide vane from different inlets as the particle density increases. This phenomenon is primarily caused by gravity. Before the particles collide with the blade, the particle trajectories in area II are farther away from the blade pressure side than in area I, and the particle trajectories in area Ⅲ are the farthest from the blade pressure side. Moreover, the particle trajectories with the density of 1800 $kg \cdot m^{-3}$ are consistent with the blade contour in area I, which leads to severe wear. The reason for this phenomenon is the minimum fluid velocity at the inlet of area I and the maximum fluid velocity at the inlet of area Ⅲ, leading to the difference axial force of particles. It can be seen from Fig. 9 (b) that the feature in the second stage guide vane under different particle densities is the same as that in the first stage guide vane at different areas. In the second stage guide vane, the particle trajectories in area I and area II are more consistent than in the first stage guide

vane under different densities. This is because particles obtain the circumferential velocity in the first stage and second stage impeller, the fluid velocity at the inlet of area I and area II is small. Inertia dominates the particle trajectories after entering the guide vane. Therefore, the wear on the blade of the second stage guide vane is more serious than that of the first stage guide vane, especially with high particle density.

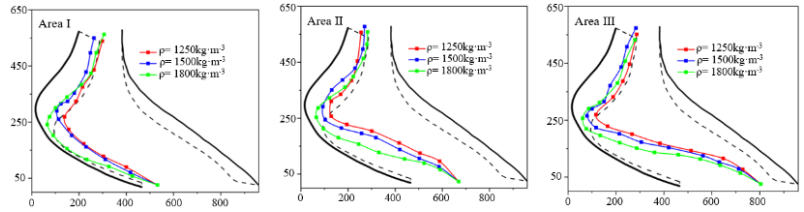

(a) First stage guide vane

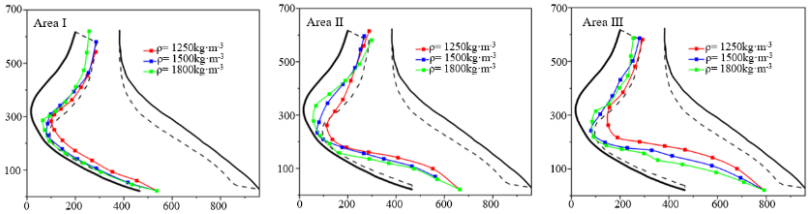

(b) Second stage guide vane

Figure 9. Particle trajectories with different densities

3.2.2 Particle distribution

Figure 10 shows the cylindrical particle number distribution at the guide vane inlet under different densities. It can be observed that the position of the flow passage components has a little effect on the particle distribution at the inlet under different densities, and the particles primarily flow into the guide vanes from area III. As the density increases, the number of cylindrical particles entering from area I gradually increases. This is because particles are weakened by the static and dynamic interference between the impeller and the guide vane as the density increases.

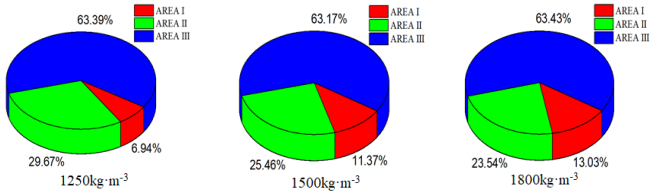

(a) First stage guide vane

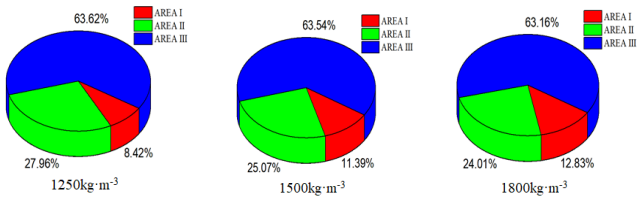

(b) Second stage guide vane

Figure 10. Particle distribution under different densities at inlet

Figure 11 illustrates the cylindrical particle number distribution at the outlet of the guide vane under different densities. It is observed that, the particles mainly flow out the guide vane from area V under different densities, and the position of the flow passage components has minimal effect on the

particle distribution. With the increase of density, the number of cylindrical particles flowing out of the area Ⅶ increases. This is because the turbulent kinetic energy in area Ⅶ is large due to the change of pressure gradient, which provides energy for some particles with large density flow out of the guide vane. At area V of the first stage guide vane inlet, the distribution of the particles is less than that of the second stage guide vane.

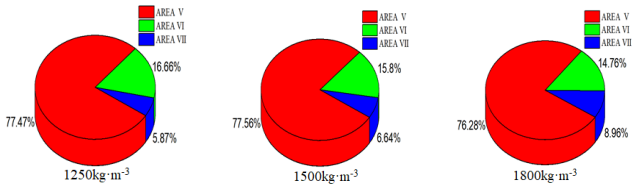

(a) First stage guide vane

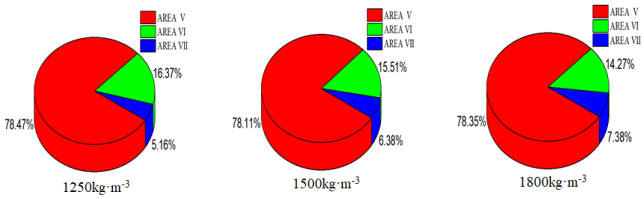

(b) Second stage guide vane

Figure 11. Particle distribution under different densities at outlet

3.2.3 Particle velocity

Figure 12 shows the cylindrical particle velocity in the guide vanes under different densities. It can be seen that the particle velocity increases first, then decreases, and finally increases again. Wang *et al.* [22] also found this law through numerical simulation and explained that the particle acceleration is caused by inertia, and particles decelerate after collision with the guide vane. In the first stage guide vane, the particle velocity reaches the highest at the second layer and the lowest at the fourth layer. The particle velocity with the density of 1250 kg·m^{-3}, 1500 kg·m^{-3}, and 1800 kg·m^{-3} at the last layer is 30.22 %, 31.13 %, and 36.45 % lower than that in the first layer, respectively. In the second stage guide vane, the particle velocity reaches the highest at the second layer and the lowest at the fourth layer. The particle velocity with the density of 1250 kg·m^{-3}, 1500 kg·m^{-3}, and 1800 kg·m^{-3} at the last layer is 33.09 %, 35.19 %, and 38.92 % lower than that at the first layer, respectively. It can be seen that the positions of the particle maximum velocity are consistent under different flow components. The velocity loss of particles through the guide vanes increases as the density increases. Compared with the first stage guide vane, the velocity loss is large in the second stage guide vane.

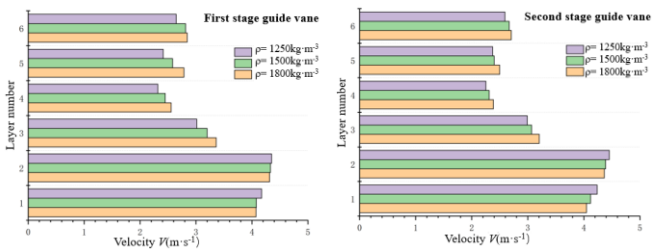

Figure 12. Particle velocity

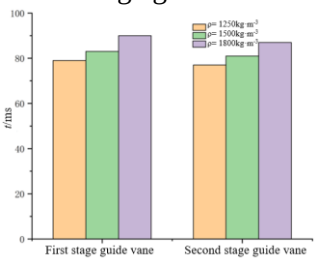

Figure 13. The particle passing time

3.2.4 The time of particles passing through the guide vanes

The time of particles flowing from the guide vane inlet to outlet is counted, and the average value is taken as the time when the particles pass through the guide vanes. Figure. 13 shows the time of cylindrical particles passing through the guide vane under different densities. It can be observed that the passing time of the cylindrical particles with the densities of 1250 $kg \cdot m^{-3}$, 1500 $kg \cdot m^{-3}$, and 1800 $kg \cdot m^{-3}$ in the first guide vane are 79ms, 83ms, and 90ms, respectively. The particles passing time in the second stage guide vane are 77ms, 81ms, and 87ms, respectively. With the increase of particle densities, the passing time of particles through the guide vanes increases. This is because the larger the density is, the closer the particles to the blade are (as seen in Fig. 9), which makes the collision more easily between particles and the blade pressure side. Compared with the first stage guide vane, the passing time of particles through the second stage guide vane is shorter.

3.3. Particle movement law under different concentrations

3.3.1 Particle trajectories

Figure 14 shows the cylindrical particle trajectories under different concentrations. It is evident that the cylindrical particles move along the blade pressure side. As shown in Fig. 14 (a), when particles enter the guide vane from different inlets, the particle trajectories get closer to the pressure side with the increase of concentration. The reason for this phenomenon is that the energy provided by the fluid to the single particle is reduced when the particle number increases. In the area I, the particle movement is consistent. This is owing to the number of particles flowing from the area I into the guide vane is less than other inlets (as seen in Fig. 10), which leads to fewer collisions between particles and less energy loss. In Figure 14 (b), it is observed that the particle trajectories move closer to the blade pressure side with the increase of concentrations. Compared with the first stage guide vane, the particle trajectories in the second stage guide vane are smaller from the blade pressure side, especially the particle trajectories in area I. This is due to the particles in the second stage guide vane obtaining the circumferential velocity in the first stage and second stage impeller. But the energy provided by the fluid to the single particle is not enough to lift the particle upward, so the particles move along the pressure side under the action of circumferential velocity. This means that the blades in the second stage guide vane are more prone to wear caused by particle impact.

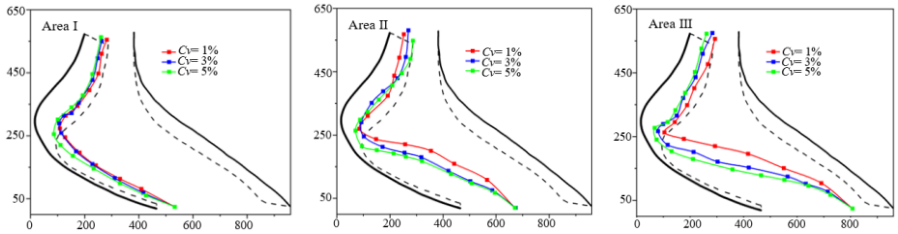

(a) First stage guide vane

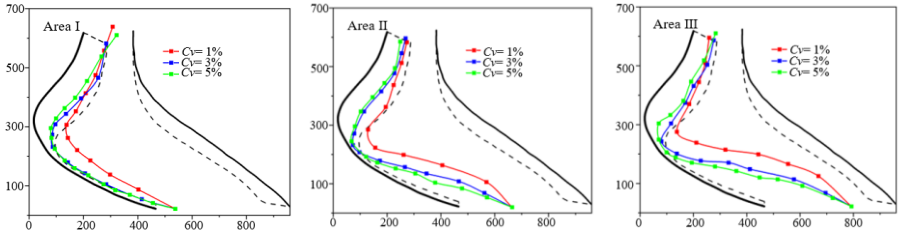

(b) Second stage guide vane

Figure 14. Particle trajectories under different concentrations

3.3.2 Particles velocity

Figure 15 shows the velocity of cylindrical particles under different concentrations in the guide vanes. It can be seen that the particle velocity increases first, then decreases, and finally increases again under different concentrations. In the first stage guide vane, the particle velocity reaches the maximum at the second layer and the minimum at the fourth layer. The particle velocity of cylindrical particles under concentrations of 1 %, 3 %, and 5 % at the last layer is 33.55 %, 31.13 %, and 34.70 % lower than those at the first layer, respectively. In the second stage guide vane, the particle velocity reaches the maximum at the second layer and the minimum at the fourth layer. The particle velocities of cylindrical particles under concentrations of 1 %, 3 %, and 5 % at the last layer are 32.60 %, 35.19 %, and 35.28 % lower than those at the first layer, respectively. It is evident that the total velocity loss of particles increases with the increase of particle concentrations. Compared with the first stage guide vane, the velocity loss in the second stage guide vane under concentrations of 1% and 5% is the same. This is because the fluid dominates the particle velocity when the concentration is lowest. When the concentration is the highetst, the accumulation of particles in the middle of the guide vane flow channel restricts the particle motion.

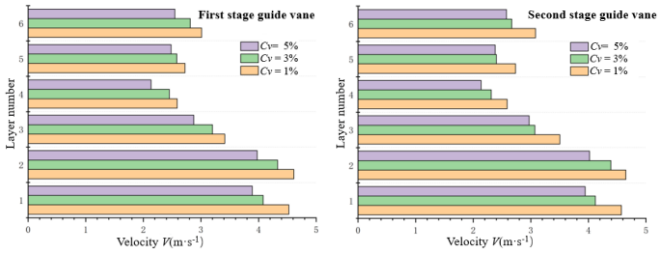

Figure 15. Particle velocity

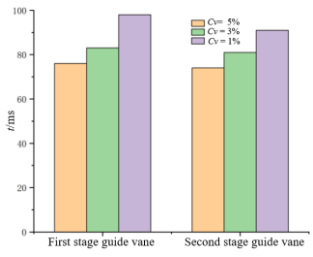

Figure 16. The particle passing time

3.3.3 The time of particles passing through the guide vane

Figure. 16 presents the passing time of cylindrical particles under different concentrations through the guide vanes. It can be observed that the passing time for cylindrical particles with a

concentration of 1 %, 3 %, and 5 % in the first stage guide vane is 76ms, 83ms, and 98ms, respectively. The passing time of the second stage guide vane is 74ms, 81ms, and 91ms, respectively. As the particle concentration increases, the passing time of particles through the guide vanes increases. This is because the particle velocity becomes lower with the increase of concentrations and the particle accumulation in the middle of the guide vane flow channel deteriorates. Comparatively, the passing time of particles through the second guide vane is shorter than through the first stage guide vane.

3.4. Particle movement law with different shapes

3.4.1 Particle trajectories

Figure.17 illustrates the particle trajectories with different shapes. It can be found that the particles predominantly move along the blade pressure side under different shapes. As shown in Fig. 17 (a), the trajectories of cylindrical particles at the inlet exhibit a greater deviation from the blade pressure side than that of the spherical particle. Because of the large aspect ratio of cylindrical particles, the gradient of fluid velocity at the guide vane inlet causes particle rotation, and the pressure difference of flow field makes the cylindrical particles move to the side with high fluid velocity. It can be seen from Fig. 17 (b) that the cylindrical particle trajectories in area I are closer to the blade pressure side than that in other areas. The reason for this phenomenon is that the fluid velocity difference at the inlet has little effect on particle trajectories. The cylindrical particle trajectories are primarily affected by the circumferential velocity of particles obtained in the first stage and second stage impeller. Combined with Fig. 17 (a) and Fig. 17 (b), cylindrical particles are more easy to collide with the middle of the guide vane than spherical particles. Therefore, cylindrical particles cause more serious wear in the middle of the guide vane flow channel.

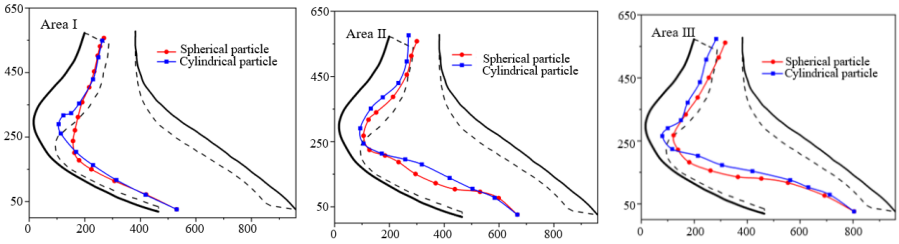

(a) First stage guide vane

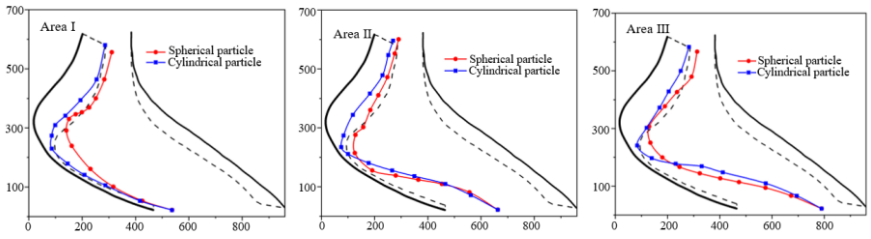

(b) Second stage guide vane

Figure 17. Particle trajectories under different shapes

3.4.2 Particle distribution

Figure 18 shows particle distribution of spherical particles at the guide vane inlet. Combined with Fig. 10, it becomes evident that the particles mainly flow into the guide vane from area III under different shapes, and the particles entering the guide vane from area I are less. The position of the flow

passage components has a little effect on the particle distribution under different shapes at the inlet. Compared with spherical particles, the number of cylindrical particles flowing into the guide vanes from area III is large. This is because the fluid velocity is fast at area III, and the cylindrical particles move to the side with fast fluid velocity under the action of pressure gradient difference. Compared with the first stage guide vane, both cylindrical particles and spherical particles show a larger number of particles flowing into the second guide vanes from area III, which is due to that the fluid velocity in the second stage guide vane at area III is large compared to the first stage guide vane.

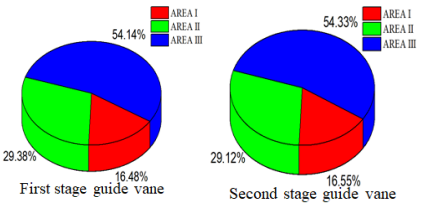

Figure 18. Particle distribution at inlet

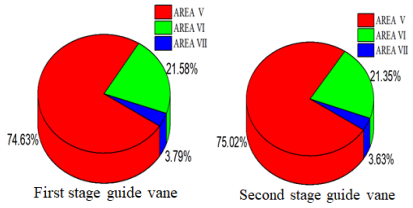

Figure 19. Particle distribution at outlet

Figure 19 depicts the number distribution of spherical particles at the guide vane outlet. Combined with Fig. 11, it is apparent that the particles primarily flow out of the guide vane from area V under different particle shapes while the number of particles flowing out from area VII is relatively small. The particle distribution under different shapes at the outlet is less affected by the position of the flow passage components. Compared with spherical particles, the number of cylindrical particles that flow out of the guide vane from area V are more. And the number of cylindrical particles that flow out of the guide vane from area VII is greater than that of the spherical particles.

3.4.3 Particle velocity

Figure 20 shows the average velocity of spherical particles and cylindrical particles at different positions in the guide vanes. It can be seen that the particle velocity all increases first, then decreases, and finally increases again under different shapes. In the first stage guide vane, the maximum of particle velocity is at the second layer and the minimum is at the fourth layer. Compared with the velocity at the first layer, the velocity of spherical particles at the last layer decreases by 32.42 %. And it is 30.88% for cylindrical particles. In the second stage guide vane, the maximum of particle velocity is at the second layer and the minimum is at the fourth layer. Compared with the velocity at the first layer, the velocity of spherical particles at the last layer decreases by 35.77%. For cylindrical particles, it is 35.19 %. It can be seen that the velocity loss of cylindrical particles is smaller than that of the spherical particles, which is due to the cylindrical particles will move along the surface with minimum resistance during the flow. Compared with the first stage guide vane, the particle velocity loss in the second stage guide vane is larger.

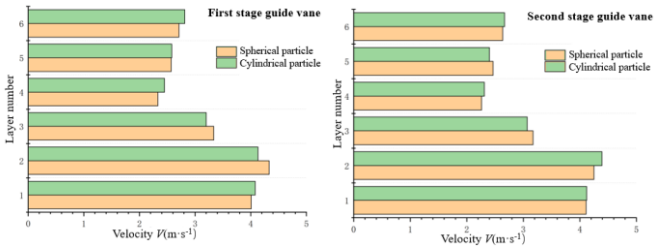

Figure 20. Particle velocity

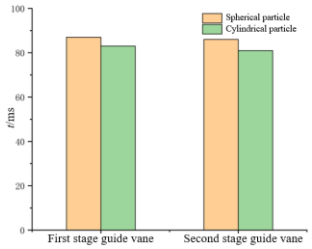

Figure 21. The particle passing time

3.4.4 The time of particles passing through the guide vane

Figure 21 shows the time of spherical particles and cylindrical particles to pass through the guide vanes. It can be seen that the spherical particles take 87ms to pass through the first stage guide vane, while the cylindrical particles take 83ms. The time of the spherical particles passing through the second stage guide vane is 86ms, and it is 81ms for cylindrical particles. Contrary to the particle backflow performance, the time of non-spherical particles passing through the guide vane is shorter than that of the spherical particles [23]. Compared with spherical particles, the time of cylindrical particles passing through the guide vane is shorter, which is related to the low particle velocity loss. Moreover, the time of particles passing through the second stage guide vane for both spherical and cylindrical particles is shorter than the first stage guide vane. This is because the particles obtain energy in the first stage and second stage impeller before they flow into the second stage guide vane, so the particle velocity in the second stage guide vane inlet is faster than that in the first stage guide vane.

4. Conclusions

The high-speed photography technology is used to investigate the energy characteristics, particle trajectories, particle distributions, particle velocity, and time of particles passing through the guide vane in the pump under different physical parameters. The significant conclusions are below.

(1) With the increase of cylindrical particle densities, the particles are more likely to move the blade pressure side of the guide vane, which leads to wear at the blade pressure side. And the wear at the blade pressure side in the second stage guide vane is more serious than that in the first stage guide vane. The particles primarily flow into the guide vanes from the suction side. The particles flowing into the guide vanes from the pressure side are the least, and the number of particles increases with densities. The particles mainly flow out of the guide vanes from the pressure side. The particles flowing out of the guide vanes from the suction side are the least and the number of the particles increases with densities. As the particle density increases, the velocity loss of particle passing through the guide vanes increases, and the time of particle passing through the guide vanes increases. Therefore, the pump efficiency reduces with the increase of densities.

(2) With the increases of cylindrical concentrations, the particles move closer to the blade pressure side of the guide vane, leading to wear at the blade pressure side. And the wear at the blade pressure side in the second stage guide vane is more serious than that in the first stage guide vane. As the particle concentration increases, the total velocity loss of particles increases, and the time of particles passing through the guide vanes increases, which results in pump efficiency reduction.

(3) Under different particle shapes, the cylindrical particles are more easy to wear the middle of the guide vane than the spherical particles. The particles mainly flow into the guide vanes from the suction side, and the cylindrical particle number flowing into the guide vanes from the suction side is larger than that of the spherical particles. The particles primarily flow out of the guide vanes from the pressure side, and the cylindrical particles number flowing out of the guide vanes from the pressure side is larger than that of the spherical particles. Compared with spherical particles, the velocity loss of cylindrical particles is smaller in the guide vane, and the time of cylindrical particles passing through the guide vane is shorter, so the pump efficiency is better when pump conveys cylindrical particles two-phase flow.

Acknowledgments

The authors gratefully acknowledge the support from the National Natural Science Foundation of China (No. 51979124)

Nomenclature

n_s – specific speed
Q_d – nominal flow rate [$m^3 \cdot h^{-1}$]
H – pump head [m]
n – rotating speed [$r \cdot min^{-1}$]
d – the bottom diameter of cylindrical particle [mm]
h – the height of cylindrical particle [mm]
η – pump efficiency
P – pump power [kW]
ρ – particle density [$kg \cdot m^{-3}$]
C_v – volume fraction of particles
ΔZ – Inlet and outlet height difference [m]
P_{out} – Total pressure of the pump outlet [Pa]
P_{in} – Total pressure of the pump inlet [Pa]
v_2 – Average velocity of pump outlet [$m \cdot s^{-1}$]
v_1 – Average velocity of pump inlet [$m \cdot s^{-1}$]
ρ_p – Solid phase density [$kg \cdot m^{-3}$]
V_p – Solid phase volume [m^3]
V_f – Liquid phase volume [m^3]
g – Acceleration of gravity [$m \cdot s^{-2}$]
Q – Inlet flow [$m^3 \cdot h^{-1}$]

References

[1] Kang, Y.J., Liu, S.J., Summary of research on lifting system of deep sea mining, *Journal of Mechanical Engineering*, 57(2021), 20, pp. 232-243.
[2] Ahmad, K., *et al.*, Computation and experimental results of wear in a slurry pump impeller, *Proceedings of the Institution of Mechanical Engineers, Part C: Journal of Mechanical Engineering Science*, 200(1986), 6 pp. 439-445.
[3] Oka, Y. I., *et al.*, Practical estimation of erosion damage caused by solid particle impact: Part 1: Effects of impact parameters on a predictive equation, *Wear*, 259(2005), 1-6, pp. 95-101.
[4] Noon, A. A., Kim, M. H., Erosion wear on centrifugal pump casing due to slurry flow, *Wear*, 364(2016), pp. 103-111.
[5] Tarodiya, R., Gandhi, B. K., Numerical investigation of erosive wear of a centrifugal slurry pump due to solid-liquid flow, *Journal of Tribology*, 143(2021), 10.
[6] Zhang, D, S., *et al.*, Numerical simulation and optimization of solid-liquid two-phase flow in a back-swept axial-flow pump, *Thermal Science*, 21(2017), pp. 64-64.
[7] Beauchesne, C., *et al.*, Development & large scale validation of a transient flow assurance model for the design & monitoring of large particles transportation in two phase (liquid–solid) riser systems, Offshore Technology Conference, OnePetro, 2015.
[8] Takano, S., *et al.*, Experimental Studies of Pressure Loss for Large Particle Slurry Transport in Oscillated Pipe for Subsea Mining, International Conference on Offshore Mechanics and Arctic Engineering, American Society of Mechanical Engineers, 2017, Vol. 57724, pp. V006T05A013.
[9] Masanobu, S., *et al.*, Experimental Studies of Pressure Loss in Inclined Pipe in Slurry Transport for Subsea Mining, International Conference on Offshore Mechanics and Arctic Engineering, American Society of Mechanical Engineers, 2015, Vol. 56543, pp. V006T05A007.
[10] Ghosh, A., Vertical Lift Study for Harvesting of Seabed Minerals for Deep Sea Mining, Ph.D. thesis, National University of Singapore, Singapore, 2017.
[11] Deng, L., *et al.*, Particle distribution and motion in six-stage centrifugal pump by means of slurry experiment and CFD-DEM simulation, *Journal of Marine Science and Engineering*, 9(2021), 7, pp. 716.
[12] Hu, Q., *et al.*, CFD-DEM coupled simulation and experimental study of deep sea lifting mine pump under extreme working conditions, *The Chinese Journal of Nonferrous Metals*, 31(2021), 10, pp. 2926-2937.

[13] Tan, M., G., *et al.*, Study on particle motion characteristic in mining lifting pump under runaway condition, *Journal of Huazhong University of Science and Technology (Natural Science Edition)*, (2022), pp. 1-8.
[14] Hu, Q., *et al.*, CFD-DEM simulation of backflow blockage of deep-sea multistage pump, *Journal of Marine Science and Engineering*, 9(2021), 9, pp. 987.
[15] Guan, Y., J., *et al.*, Ore particle backflow performance in the deep-sea mining slurry pump, *Journal of Harbin Engineering University*, 42(2021), 11, pp. 1557-1565.
[16] Sun, X., L., *et al.*, Influence of mineral particle size on wear characteristics of deep-sea mining lifting pump, *Journal of Drainage and Irrigation Machinery Engineering*, 40(2022), 11, pp. 1097-1103.
[17] Wang, R., *et al.*, Influence on the Solid-Liquid Two-Phase Flow from Cross-Section Area of Slurry Pumps for Deep-Sea Mining, *China Ocean Engineering*, 36(2022), 3, pp. 439-450.
[18] Luo, R., C., *et al.*, Experimental studies on characteristics of coarse particle motion in different guide vanes of lifting pump for deep-sea mining, J*ournal of Central South University (Science and Technology)*, 49(2018), 12, pp. 2963-2971.
[19] Wu, X., F., *et al.*, Visualization test on solid-liquid two-phase flow in multistage pump, *Journal of Drainage and Irrigation Machinery Engineering*, 39(2021), 12, pp. 1270-1277.
[20] Chen, J., *et al.*, Experiment on vibration characteristics of double-suction centrifugal pump under multiple working conditions, *Journal of Jiangsu University (Natural Science Edition)*, 42(2021), 5, pp. 526-532+553.
[21] Dong, X., R., *et al.*, Simulation analysis and experimental study on flow/pressure regulating valve in Sanhekou Water Control Project, *Water Resources and Hydropower Engineering*, 51(2020), 9, pp. 114-132.
[22] Wang, R., *et al.*, Impact of Particle Sizes on Flow Characteristics of Slurry Pump for Deep-Sea Mining, *Shock and Vibration*, 2021(2021), pp. 1-13.
[23] Guan, Y., J.,*et al.*, Ore particle backflow performance in the deep-sea mining slurry pump, *Journal of Harbin Engineering Univeristy*, 42(2021), 11, pp. 1557-1565.

Submitted: 13.05.2023.
Revised: 22.08.2023.
Accepted: 29.08.2023.